

# Neural-Network-Based Adaptive Sampling of Three-Dimensional-Object Surface Elastic Properties

Ana-Maria Cretu, *Student Member, IEEE*, and Emil M. Petriu, *Fellow, IEEE*

**Abstract**—The paper discusses an adaptive-sampling technique for dimensionality reduction of the set of probing points in the measurement of nonuniform elastic properties of three-dimensional (3-D) objects. Two self-organizing neural-network architectures are compared for this purpose: the neural-gas network and the Kohonen self-organizing map (SOM).

**Index Terms**—Adaptive systems, neural-network applications, robot tactile systems, self-organizing feature maps, topology.

## I. INTRODUCTION

**L**ASER OR RANGE scanners are capable of providing accurate data on the geometrical properties of the objects. However, they are not capable of providing any information about the elasticity of the objects, which is an important parameter for the computer-aided design (CAD)/computer-aided manufacturing (CAM), quality control, and reverse engineering of elastic-material components, as well as for many dexterous manipulation applications such as robotic assembly, telerobotics, remote medical examination of patients, medical robotics, interactive virtual environments for training, and the computer-game industry [1]–[3]. Moreover, the recovery of the elastic-material properties, which by definition implies touching each point of interest on the explored object surface and then conducting a strain–stress relation recovery measurement on each of the touched points, is a very time-consuming operation. This explains the considerable interest in finding fast sampling procedures for the robotic measurement of the elastic properties of three-dimensional (3-D) object surfaces, which imply the ability to minimize the number of the sampling points by selecting only those points that are relevant to the elastic characteristics of an object. This paper proposes a nonuniform adaptive-sampling algorithm of the object’s surface, which exploits the self-organizing neural-networks’ ability to find an optimal finite quantization of the input space, as depicted in Fig. 1.

Manuscript received June 15, 2004; revised October 28, 2005. This work was supported in part by the Communications and Information Technology Ontario (CITO) Center of Excellence, by the Materials and Manufacturing Ontario (MMO) Center of Excellence, and by the Natural Sciences and Engineering Research Council of Canada (NSERC).

The authors are with the School of Information Technology and Engineering, University of Ottawa, Ottawa, ON K1N 6N5 Canada (e-mail: acretu@site.uottawa.ca; petriu@site.uottawa.ca).

Digital Object Identifier 10.1109/TIM.2006.870114

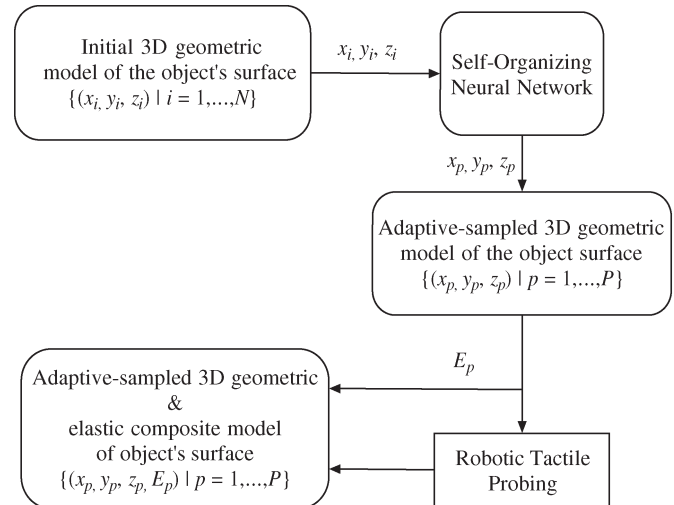


Fig. 1. Neural-network-based adaptive-sampling control of the robotic tactile probing of the elastic properties of a 3-D object surface.

## II. NONUNIFORM ADAPTIVE SAMPLING OF TACTILE DATA

The surface of 3-D objects deforms proportionally with the force applied on the normal direction to that surface. The elastic behavior at any given point  $(x_p, y_p, z_p)$  on the object surface is described by the Hooke’s law as

$$\begin{cases} \sigma_p = E_p \cdot \varepsilon_p, & \text{if } 0 \leq \varepsilon_p \leq \varepsilon_{p \max} \\ \sigma_p = \sigma_{p \max}, & \text{if } \varepsilon_{p \max} < \varepsilon_p \end{cases} \quad (1)$$

where  $E_p$  is the modulus of elasticity,  $\sigma_p$  is the stress, and  $\varepsilon_p$  is the strain on the normal direction. The modulus of elasticity  $E_p$  is measured by a tactile probe robot carried by a robot manipulator that places the tip of the probe on normal direction at each given point  $(x_p, y_p, z_p)$  of the object’s surface. The changes of the modulus of elasticity are usually correlated with the changes of the geometric shape of the surface. This means that the density of the tactile probing points should be higher in the regions with more pronounced variations in the geometric shape.

As it happens in reality, the objects modeled are usually not elastic, but they rather exhibit a viscoelastic behavior. Therefore, a range of displacements within which the object exhibits at least quasi-linear elastic behavior has to be first determined

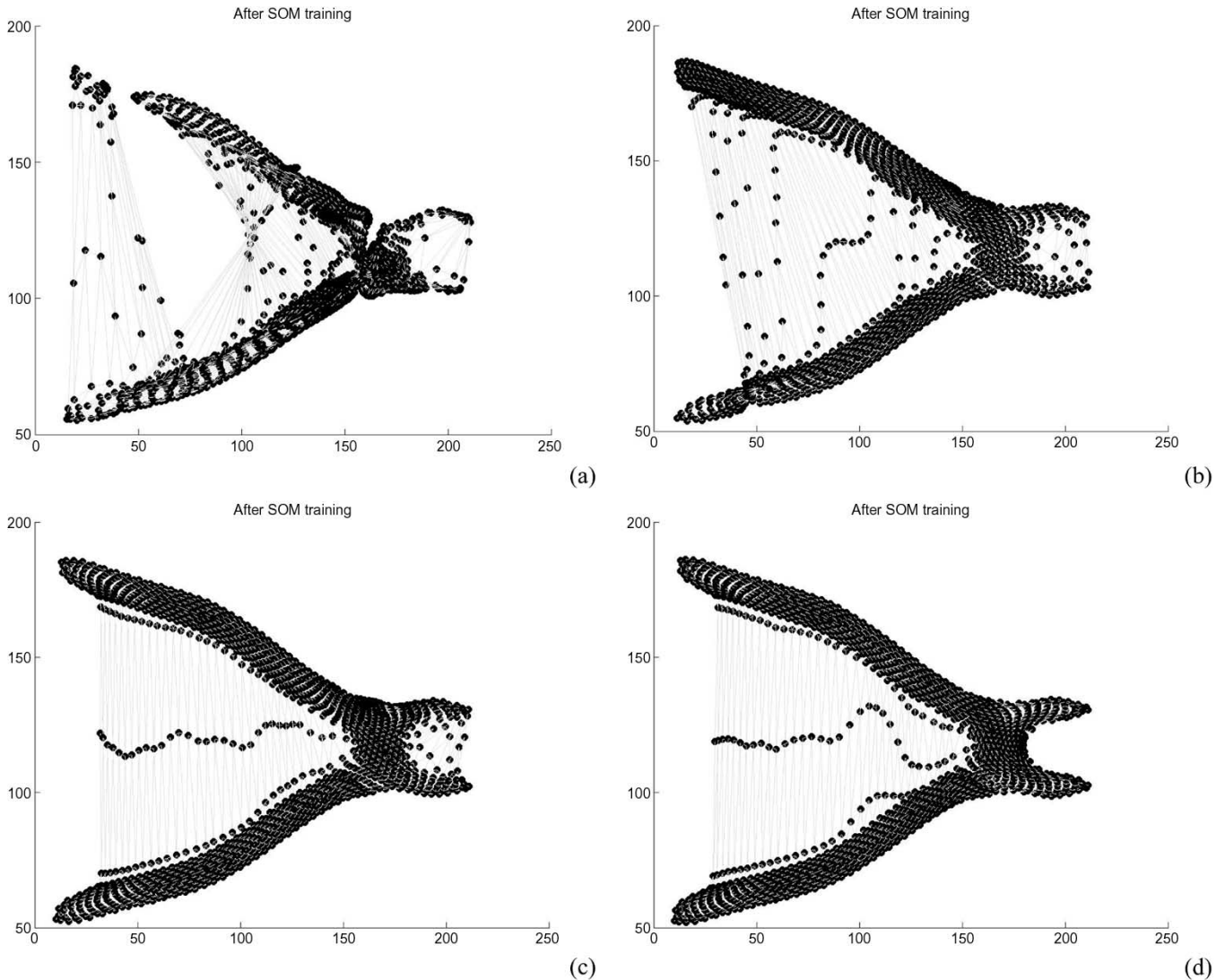


Fig. 2. SOM models for a fixed size map of  $25 \times 45$  for different training epochs. (a) Five epochs, (b) 20 epochs, (c) 100 epochs, and (d) 1000 epochs.

and, after that, the corresponding elasticity parameters obtained [4]. The range of displacements is determined experimentally by applying a force increasing linearly and with a prescribed incremented velocity on the normal direction of the surface, and by measuring the resulting displacements. As long as the measured displacements change linearly, the object is supposed to exhibit a linear elastic behavior. The modulus of elasticity is then updated using a gradient-descent method to minimize the computed deviation between experimental and simulated displacements until convergence.

Considering that we have available a highly accurate model of an object obtained using a laser or range scanner, we use a nonuniform adaptive-sampling algorithm to detect relevant points for elastic sampling based on the self-organizing neural-network ability to find an optimal finite set that quantizes the given input space. The elastic data is then collected for this set of samples. The robotic tactile probing allows the recovery of the 3-D geometric shape by registering the coordinates of the tip of the probe every time when the tactile probe detects a contact with the explored object.

### III. 3-D OBJECT MODELING USING SELF-ORGANIZING ARCHITECTURES

Two architectures are studied for the purpose of obtaining a compressed neural model that accurately reproduces the geometric properties of a 3-D object represented as a point cloud: the Kohonen self-organizing map (SOM) and the neural-gas network. The Kohonen SOM clusters the input space by assigning each neuron to a defined region. The number of inputs to each external neuron being equal to the dimension of the input space, the weight vectors can be interpreted as locations in this space. Each region is a set of locations that are closer (according to a distance measure) to the corresponding neuron than any other one. After the learning procedure, two vectors belonging to the same cluster will be projected on two close neurons in the output space. Usually, the defined topology of an SOM is a two-dimensional grid.

The low-dimensional mapping topology of the SOM is removed in the neural-gas network [5]. The neural-gas network consists of nodes that move independently over the data space while learning. The neural gas converges quickly, reaches a

lower distortion error after convergence than other methods, and obeys a gradient descent on an energy function, which is not the case of the SOM. It presents the identical quantization property of Kohonen's algorithm but does not hold the topology-preservation property, as it will be further shown.

### A. Kohonen SOM

A Kohonen SOM contains one layer of neurons and two layers of connections. Each neuron has external connections to the inputs ( $x_i$ ) and is also laterally connected to its neighbors up to a certain distance ( $c_{jk}$ , where  $k$  gives the number of neighborhoods considered).

Computations are feedforward in the first layer of connections and bidirectional in the connection layer. Each neuron in the first layer computes the weighted sum of the received inputs, while the purpose of the second layer of connections is to reinforce the activation values of "strong" neurons and decrease the activation of "weak" ones [5].

The training algorithm for an SOM is performed in three steps: weight initialization, sampling, and similarity matching and updating. The SOM is initialized linearly along its greatest eigenvectors of the input set. In each training step, one sample vector is chosen from the input set and the best matching neuron at time  $n$  is computed using the minimum Euclidean distance criterion: After finding the winning neuron, the weight vectors of the winning neuron and those of its topological neighbors are updated.

The update rule for the neurons is

$$w_j(n+1) = \begin{cases} w_j(n) + \eta(n)h_{ij}(n) \\ \quad \times [x(n) - w_j(n)], & \text{when } j \in \Lambda_{i(x)}(n) \\ w_j(n), & \text{otherwise} \end{cases} \quad (2)$$

where  $n$  denotes the discrete time,  $\eta(n)$  is the learning-rate parameter, and  $h_{ij}(n)$  is the Gaussian function representing the topological neighborhood centered around the winning neuron  $i(x)$ .

The algorithm is repeated with the sampling of the next input vector until no noticeable changes occur in the map. The learning rule is local, as the operation at each neuron only requires the knowledge of the weight associated with that neuron and the input vector. However, a nonlocal function is needed to choose the best matching neuron [6]. For the batch algorithm, the only difference is that the whole data set is run through at once and the map is updated with the effect of all samples [7].

The learning rate  $\eta(n)$  and the neighborhood function  $h_{ij}(n)$  are both time dependent. In order to ensure that the algorithm converges, it is important that the learning-rate parameter and the neighborhood radius  $\sigma$  are decreased slowly during the learning process. Although a linear function can be used to describe the decrease in time, the most popular choice is to use it in the form of a power series as

$$\sigma(n) = \sigma_0 \left( \frac{\sigma_T}{\sigma_0} \right)^{\frac{n}{T}}, \quad \eta(n) = \eta_0 \left( \frac{\eta_T}{\eta_0} \right)^{\frac{n}{T}} \quad (3)$$

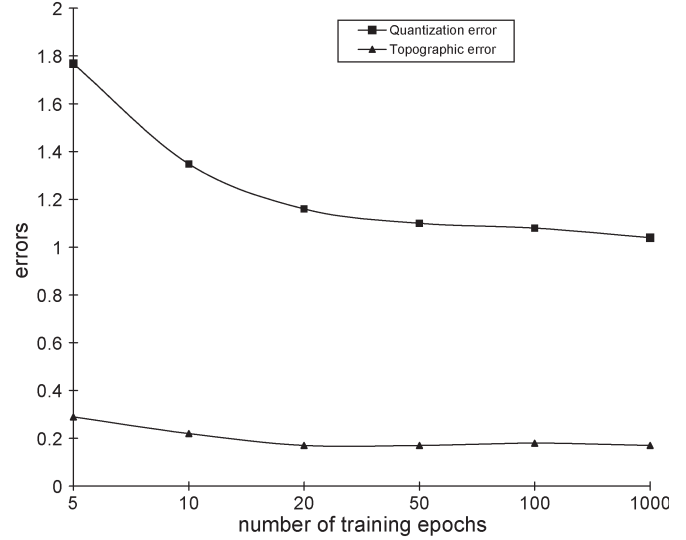


Fig. 3. SOM evolution of quantization and topographic error with the number of training epochs.

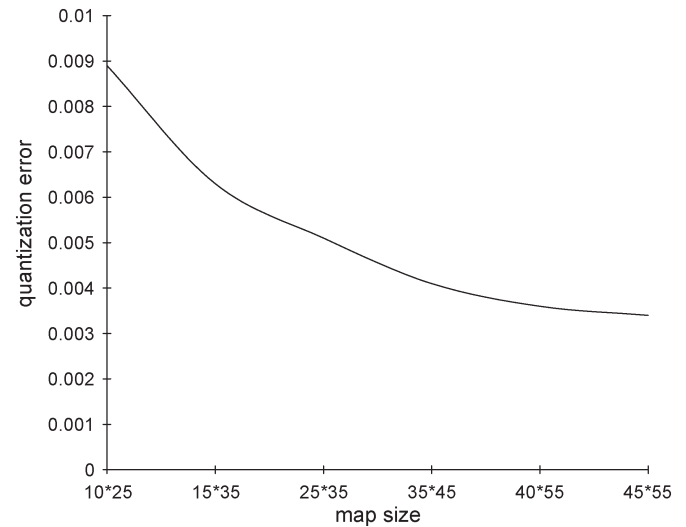


Fig. 4. Evolution of quantization error as a function of the map size for a learning rate  $\alpha_0 = 0.5$  and 10 training epochs.

where the constants  $\sigma_0$  and  $\eta_0$  are the initial values for  $\sigma(n)$  and  $\eta(n)$ ,  $\sigma_T$  and  $\eta_T$  are the final values,  $n$  is the time step, and  $T$  is the training length.

There are three main advantages of SOMs: input-space approximation, topology ordering, and density matching. An SOM transforms or preserves the similarity between input vectors from the input space into a topological closeness of neurons in the output space. Each output neuron specializes during the training procedure to react similarly to similar input vectors (belonging to a cluster in the input space) [8]. The neurons in the SOM output are topologically ordered in the sense that neighboring neurons correspond to similar regions in the input space. The SOM also preserves the data densities of the input space reasonably well, that is, regions with more data points are mapped to larger regions in the output space.

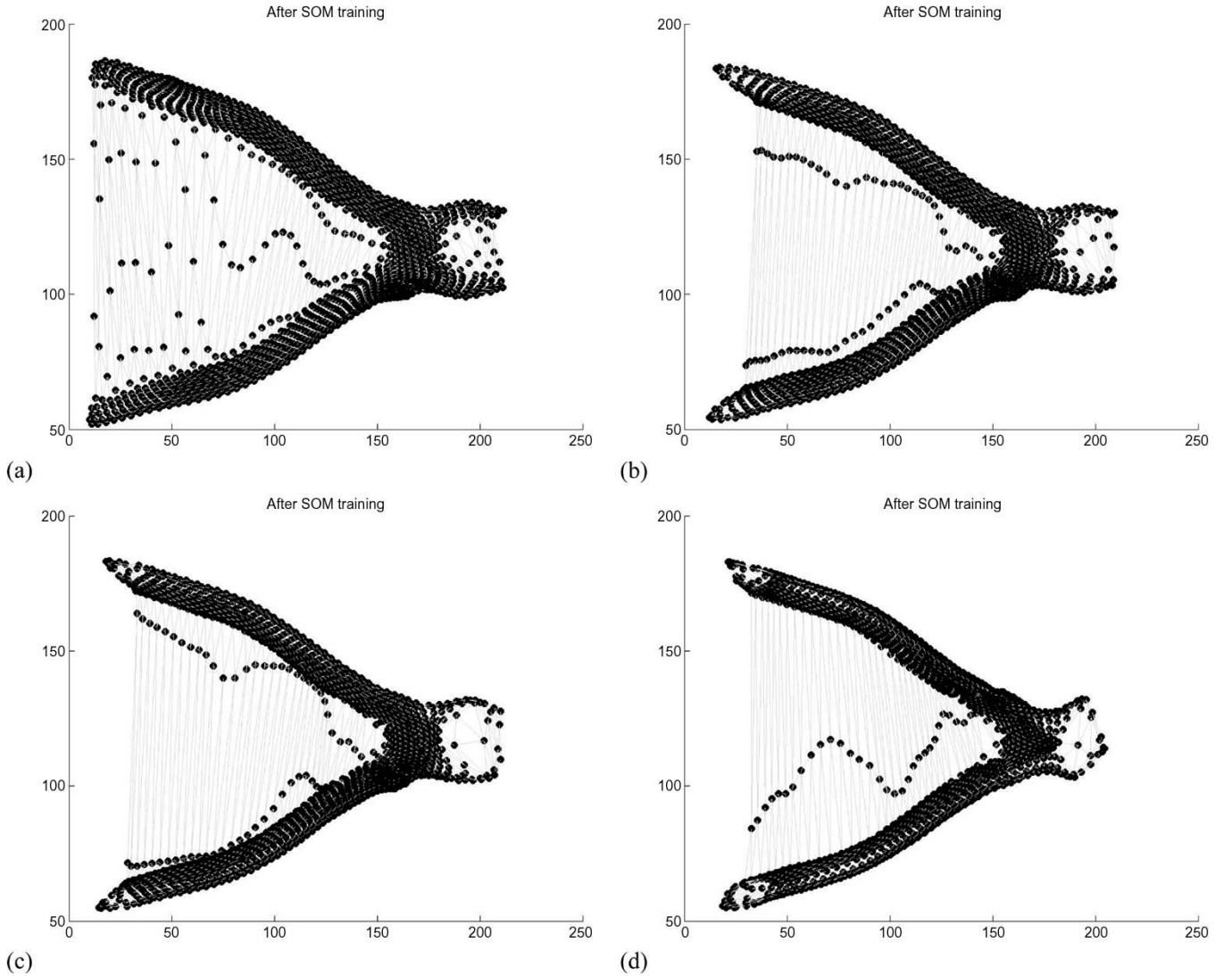


Fig. 5. Influence of neighborhood radius  $\sigma_0$  for fixed map size of  $25 \times 45$  and 500 training epochs. (a)  $\sigma_0 = 5$ ,  $q_e = 1.04$ , and  $t_e = 0.22$ ; (b)  $\sigma_0 = 500$ ,  $q_e = 1.3$ , and  $t_e = 0.1576$ ; (c)  $\sigma_0 = 1000$ ,  $q_e = 1.49$ , and  $t_e = 0.169$ ; and (d)  $\sigma_0 = 2000$ ,  $q_e = 2.1$ ,  $t_e = 0.24$ .

However, to obtain good results with a Kohonen SOM, the topology of the input space to be represented has to match to the grid used. As we previously stated, usually, maps of higher dimensions than 2 are not used since their visualization is problematic [7]. Moreover, the SOM algorithm does not have a cost function in the general case that yields the adaptation rule used as its gradient [5]. To overcome these problems, a neural-gas network releases the neurons from the two-dimensional (2-D) grid and obeys a gradient descent on a cost-function surface.

### B. Neural-Gas Network

The neural-gas network does not use a particular topology. It consists of a number of disconnected centers. However, it can be seen as a feedforward unsupervised model having one layer of neurons and one layer of connections [5]. Each neuron is connected to the input vector of the same dimension, but there are no connections between units in the neuron layer.

The neural-gas network uses the same winning neuron selection as in the SOM. However, the neurons to be adapted in the learning procedure are not selected according to a topological relation but rather according to their rank. The rank of neurons is the rank they have in an ordered list of distances between their weights and the input vector. Each time a new input vector is presented to the network, a neighborhood ranking indices list is built.

The neurons' weights are updated according to

$$w_j(n+1) = w_j(n) + \alpha(n)h_\lambda(k_j(x, w_j)) [x(n) - w_j(n)] \quad (4)$$

where  $\alpha(n) \in [0, 1]$  describes the overall extent of the modification, and  $h_\lambda$  is 1 for  $k_j(x, w_j) = 0$  and decays to 0 for higher values according to

$$h_\lambda(k_j(x, w_j)) = \exp\left(-\frac{k_j(x, w_j)}{\lambda(n)}\right). \quad (5)$$

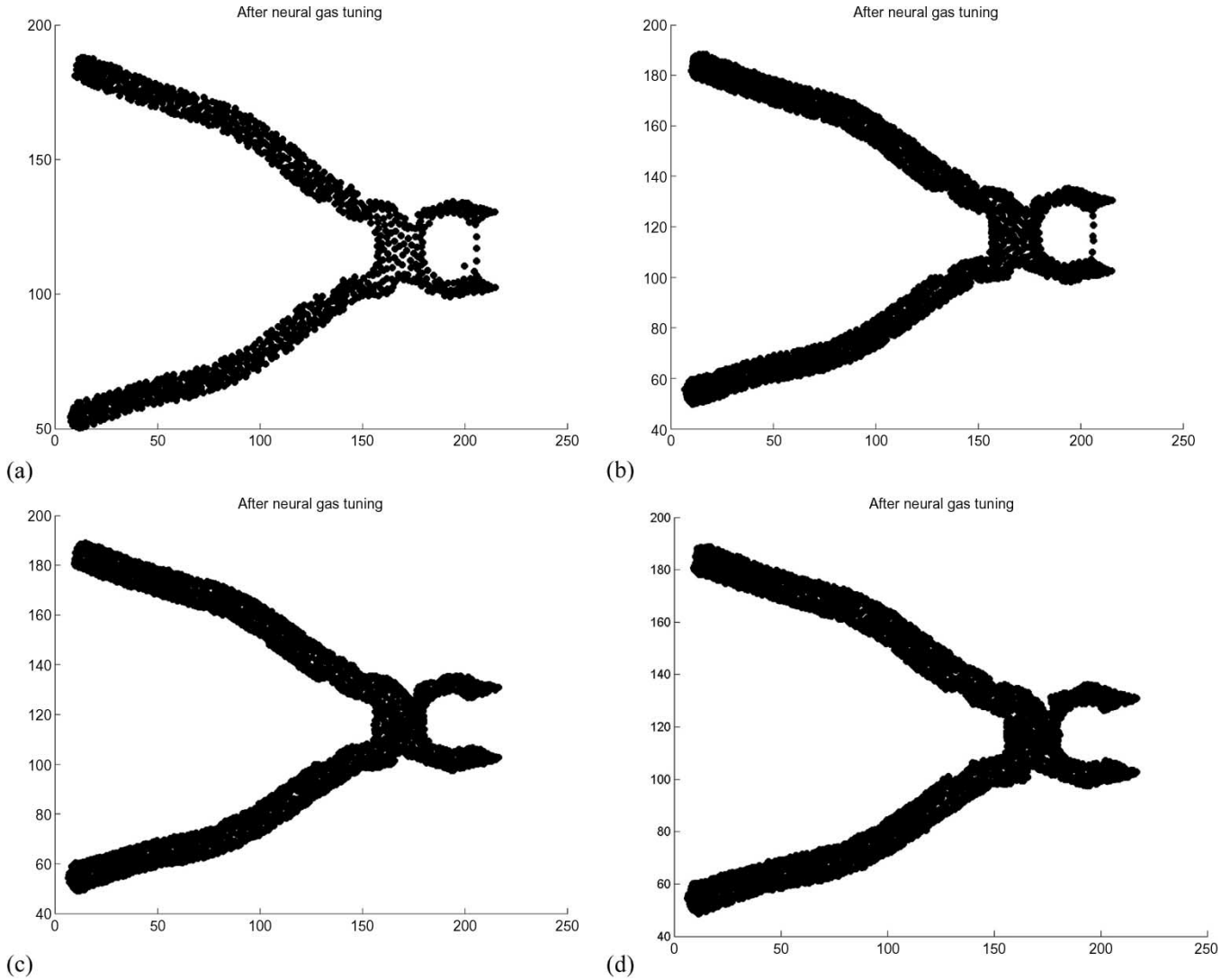


Fig. 6. Influence of the initial learning rate  $\alpha_0$  for a fixed map size  $35 \times 55$ . (a)  $\alpha_0 = 0.1$  and five epochs; (b)  $\alpha_0 = 0.1$  and 15 epochs; (c)  $\alpha_0 = 0.5$  and 15 epochs; and (d)  $\alpha_0 = 1$  and 15 epochs.

As in [3],  $k_j(x, w_j)$  is a function that represents the ranking of each weight vector  $w_j$ . If  $j$  is the closest to input  $\mathbf{x}$ , then  $k = 0$ ; for the second closest,  $k = 1$ ; and so on.

The weight initialization is done with very small values, of the order of  $10^{-5}$ . The learning rate  $\alpha(n)$  and the function  $\lambda(n)$  are both time dependent. In order to ensure that the algorithm converges, it is important that these parameters are decreased slowly during the learning process. Usually, the time dependencies in (3) are used.

A neural-gas network is claimed to have three main advantages over other methods [5]: It converges quickly, it is more accurate in that it reaches a lower distortion error after convergence, and it obeys a gradient descent on a cost function.

#### IV. SIMULATION RESULTS

As previously stated, in the context of this paper, the self-organizing architectures will be employed to obtain a com-

pressed model for the 3-D point cloud that embeds an object or a scene of objects. The weight vector will consist of the 3-D coordinates of the object's points. During the learning procedure, the model will contract asymptotically towards the points in the input space, respecting their density and thus taking the shape of the object encoded in the point cloud. Data point clouds obtained with a range scanner are used to train the network. Normalization is employed, to remove redundant information from a data set, by a linear rescaling of the input vectors such that their variance is 1.

In order to evaluate the quality of the models, some simplistic measures of the resolution and the topology are used. The quantization error [8], [9] (mapping precision) describes how accurately the neurons respond to the given data set. For example, if the reference vector of the winning neuron calculated for a given testing vector  $x_i$  is exactly the same as  $x_i$ , the error in precision is then 0. Normally, the number of data vectors exceeds the number of neurons and the precision error is thus always different from 0. It is computed as an

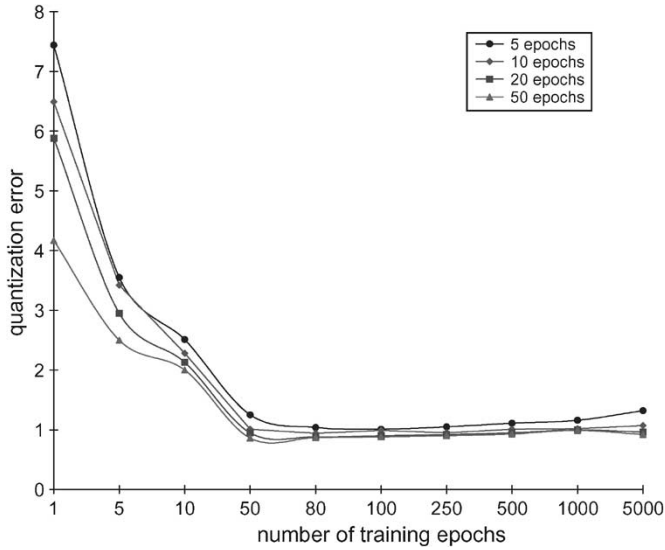


Fig. 7. Influence of  $\lambda_0$  on the quantization error for different numbers of training epochs.

average distance between each data vector and its winning neuron as

$$qe = \frac{1}{N} \sum_{j=1}^N \|x_j - w_i(x_j)\|. \tag{6}$$

The topographic error describes how well the SOM preserves the topology of the studied data set. Unlike the quantization error, it considers the structure of the map. For a twisted map, the topographic error is big even if the mapping precision error is small. The topographic error, is computed as the proportion of all data vectors for which the first and the second winning neurons are not adjacent units as

$$te = \frac{1}{N} \sum_{j=1}^N u(x_j)$$

where  $u(x) = \begin{cases} 1, & \text{if first and second winning} \\ & \text{neurons are not adjacent} \\ 0, & \text{otherwise.} \end{cases} \tag{7}$

Figs. 2 and 3 show the modeling results and the corresponding quantization and topological errors as a function of the number of training epochs for a fixed size map of  $25 \times 45$  and a value of 5, respectively, for the starting value and the final value of the radius of the neighborhood ( $\sigma_0 = 5, \sigma_T = 1$ ).

The computation time is constant and is approximately 3.4 s/epoch. The graph in Fig. 4 shows the trend of the quantization and the topographic error with the number of training epochs. As expected, the quantization error decreases with the number of training epochs, showing that the learning is improving and therefore the quality of the model is better. The topographic error remains relatively constant at a low value, indicating the SOM has a good topology-preservation capacity.

Another set of tests is conducted to show the influence of the neighborhood function choice on the learning procedure. Fig. 5 shows the influence of the initial value of neighborhood radius

$\sigma_0$ , for a fixed size map and a fixed number of training epochs on the quality of learning.

If the neighborhood is too small, the spatial map cannot be organized properly and results in large errors. It is recommended that the initial value be wide enough. However, a too large initial value leads to increases in the values of both quality parameters. From the results of the tests we performed, the best compromise between the visual quality and the values of the errors is obtained for a value of  $\sigma_0$  that is around half the dimension of the map size.

For the neural-gas counterpart, a number of simulations have been performed to show the effect of the map size in terms of computation time, storage, and quality of the model. As expected, the quality improves with the map size (Fig. 7) and the number of training epochs.

Fig. 6 shows how the learning rate affects the quality of the resulting model for different numbers of training epochs and for a fixed map size of  $35 \times 55$ . It can be seen that the quality is improving with a larger value of the initial learning rate  $\alpha_0$  (typically, the value of  $\alpha_0$  is in the interval  $[0, 1]$ ). The quantization error decreases slowly with an increase in the value of the learning rate but remains approximately constant for a threshold larger or equal to  $\alpha_0 = 0.5$ . This value is actually used for all the models.

Fig. 7 shows a decrease in the value of errors with an increase in the value of  $\lambda_0$  until the values of  $\lambda_0 = 80-100$ . After that point the error starts to increase slightly; thus, the quality deteriorates again. A value of approximately the number of neurons divided by 2 is used for the modeled objects.

From all the above-mentioned aspects, it can be concluded that the neural gas provides a relatively low error level over many training samples; it is resilient to initial starting positions and variations in parameter settings. This is gained at the expense of an increased computational load. The network is able to produce good results, even when given a limited time to converge.

Fig. 8 presents the results of training a neural-gas network with a map size of  $25 \times 45$  for 20 epochs,  $\alpha_0 = 0.5$ , and  $\lambda_0 = \text{number of neurons}/2$  and of an SOM with a map size of  $25 \times 45$  trained for 100 epochs, the initial neighborhood radius  $\sigma_0 = 5$ , and with data corrupted with different levels of noise. The initial set of 3721 points is reduced to 1125 points [10].

It takes approximately 250 s for the SOM to build a model of a sphere, while it takes approximately double for the neural gas. However, even for a larger number of training epochs (5 times more), the SOM does not reach the same accuracy as the neural gas does for data that is not very noisy (a random noise level below 0.1).

By visually comparing the results, it can be noticed that the SOM suffers from the boundary problem. The models obtained looked as if they contain cavities. By comparing the quantization error in Figs. 8 and 9, it can be seen that the neural-gas network performs better than the SOM (achieves lower levels of quantization error) for low levels of noise.

For higher levels of noise, the SOM tends to smooth the effect of noise while the neural-gas network, which has high sensitivity, follows the noisy patterns.

A comparison in terms of modeling power with nonnoisy data is presented in Figs. 10 and 11. In Fig. 10, the first

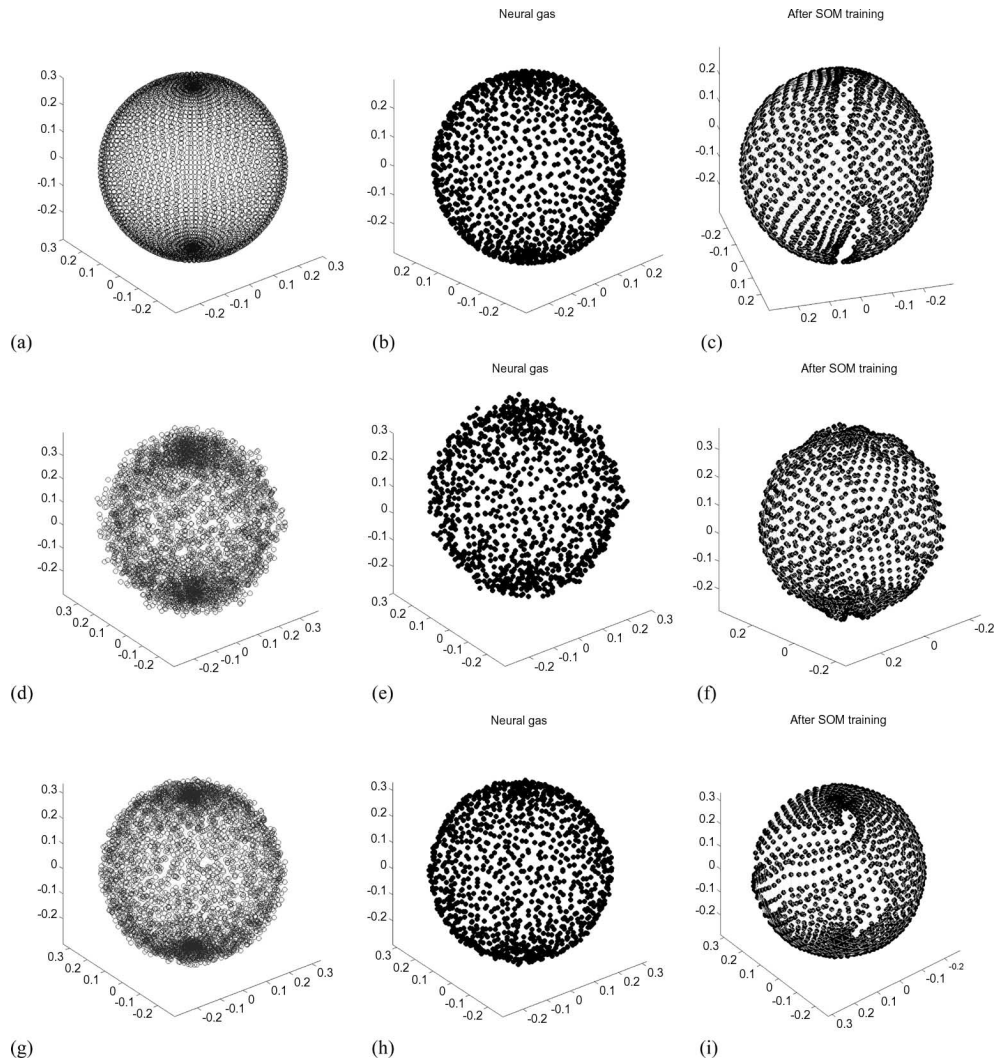


Fig. 8. Robustness to noisy training data. (a) Training data set, 3721 points. (b) Neural-gas network, error = 0.0112. (c) SOM, error = 0.0133. (d) Noisy data set, random 0–0.1. (e) Neural-gas network error = 0.0383. (f) SOM, error = 0.0266. (g) Noisy data set, random 0–0.04. (h) Neural-gas network error = 0.0224. (i) SOM, error = 0.0241.

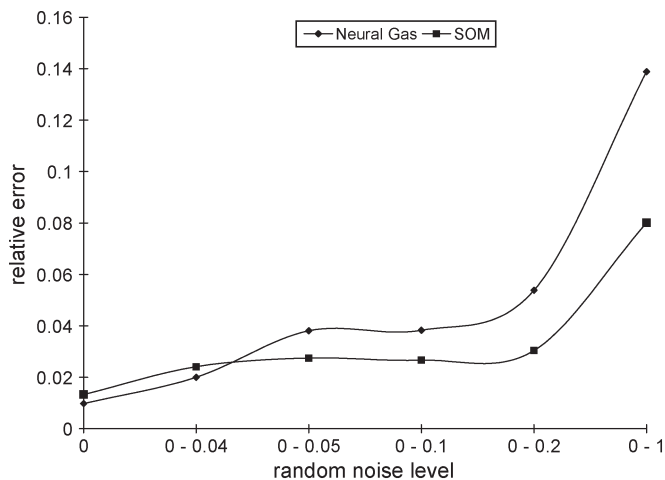


Fig. 9. Evolution of relative error in presence of a random noise.

column presents three views of a point cloud of 19 080 points representing a face, obtained using a range scanner. The second column presents the compressed model of 1152 points

obtained using the neural gas, and the last column presents the compressed model of 1152 points obtained using the SOM, deliberately chosen the same in order to compare their modeling capabilities.

In Fig. 11, different models are used to compare the qualitative aspects of the two models. The map sizes are equal for both networks. The first column represents the range data, the second presents the corresponding neural-gas model, and the last presents the SOM model.

For 14 914 points of the model of bolts in Fig. 3(a), it takes 24 min to build an SOM and 11 min to build the neural-gas model for the same map size of  $25 \times 35$ . The time to obtain the neural-gas model is significantly longer. This proportion of time is observed in almost all models.

Both neural-network architectures are able to compress the initial model with the desired degree of accuracy. For example, the 16 851 points of the baby face in Fig. 11(e) are compressed to 1152 points in both neural models.

The number of points can be further reduced by reducing the map size. However, there is a compromise to be made between

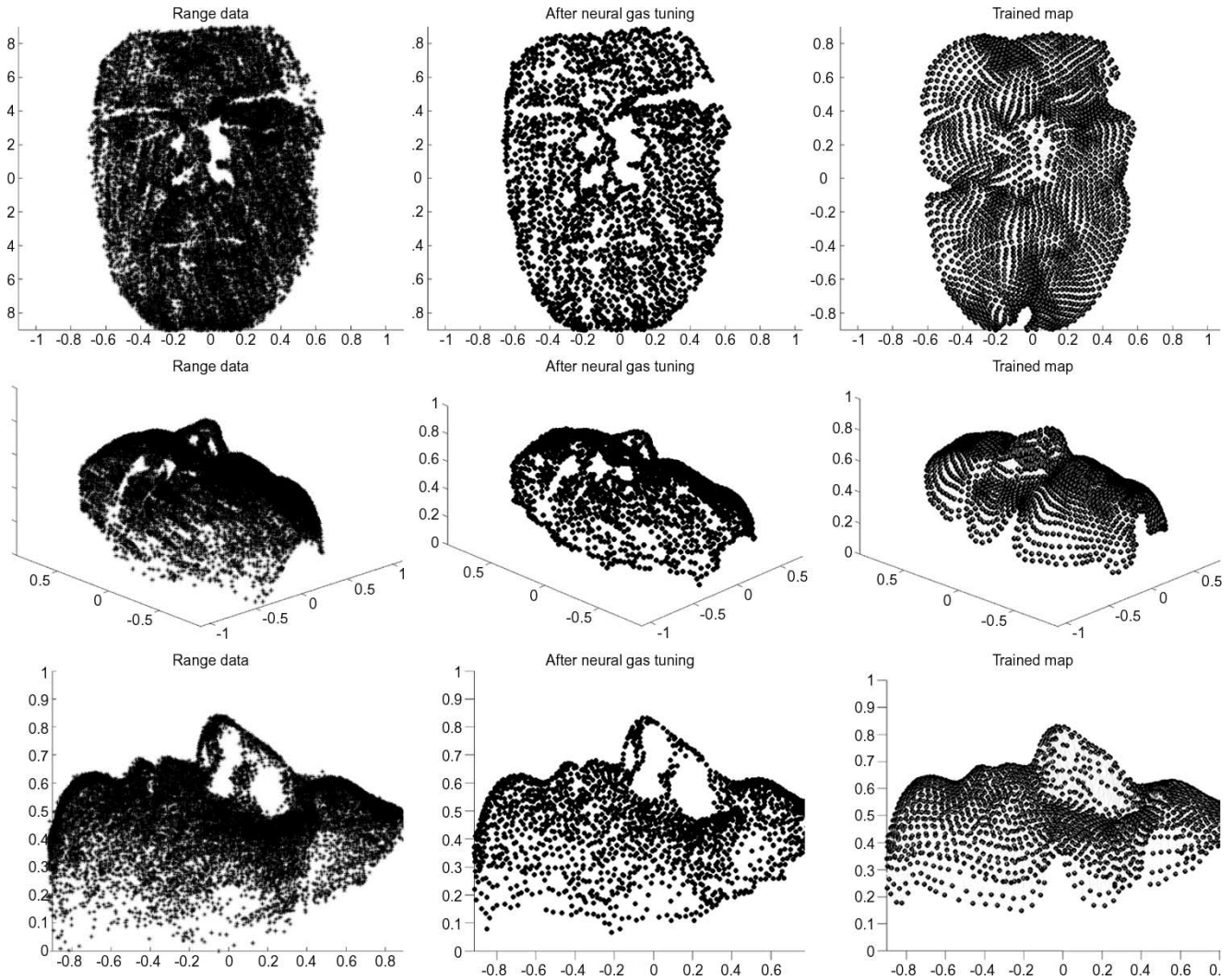


Fig. 10. Face model for a fixed map size of  $25 \times 45$ .

the quality of the resulting compressed neural model and the map size.

The same property makes it easy for the neural-gas network to model an entire scene of objects and makes it impossible for the SOM model, as depicted in Fig. 11. Such a scene can subsequently be split in the component objects using, for example,  $k$ -means clustering.

For both neural architectures, the quality is improving with the number of training epochs. As visually seen in Figs. 10 and 11 the quality of the neural-gas model appears to be better. Because of the boundary problem, the SOM models are to be avoided for nonnoisy data.

## V. CONCLUSION AND FURTHER DEVELOPMENTS

The paper discusses two self-organizing neural-network architectures, the neural-gas network and the Kohonen SOM, used for the adaptive sampling and the reduction of the dimensionality of the set of probing points in the robotic tactile measurement of the elastic properties of 3-D objects. The representation obtained by the two self-organized architectures is a compressed model with the desired level of accuracy

that preserves the geometric properties of the objects and samples more points for the areas of high density, due to the topological-preservation properties of the self-organizing neural networks.

The discussed sampling technique will be incorporated in a multisensor robotic scanning system for the recovery of the geometric shape and elastic-material properties of 3-D physical objects. The system will consist of a robot manipulator carrying a tactile probe and an attached video camera. The structured-light approach [11] will be used to provide a second set of measurements of the 3-D shape of the object. An original pseudorandom encoded grid pattern [12] will facilitate the solving of the point identification problem, as it allows for an absolute identification of both grid coordinates of any node projected on an object's surface. The resulting geometric model of the 3-D object's shape will be calibrated against the high-resolution laser-scanned model.

A multisensor fusion technique will be used to integrate the geometric and tactile measurements into a composite 3-D object model. We will investigate both deterministic and neural-network methods for the implementation of this multisensor fusion system [13], [14]. A task-specific decision-making

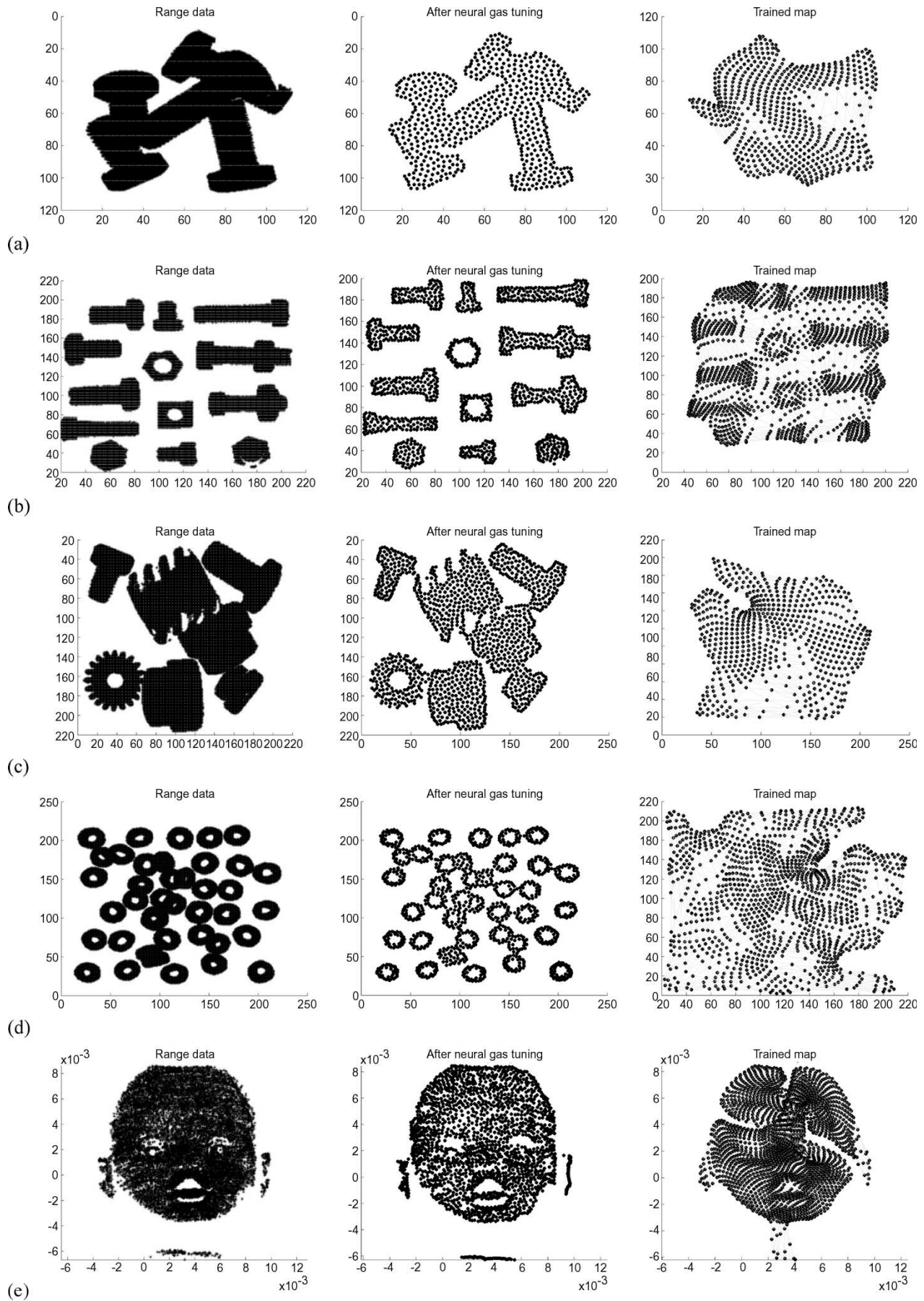


Fig. 11. Qualitative comparison between neural gas and SOM models.

process will guide the incremental refinement of the environment model [15].

#### REFERENCES

- [1] P. Allen, "Integrating vision and touch for object recognition tasks," *Int. J. Rob. Res.*, vol. 7, no. 6, pp. 15–32, 1988.
- [2] S. J. Lederman, R. L. Klatzky, and D. T. Pawluk, "Lessons from the study of biological touch for robotic haptic sensing," in *Advanced Tactile Sensing for Robotics*, H. R. Nicholls, Ed. Singapore: World Scientific, 1992.
- [3] T. Itoh, K. Kosuge, and T. Fukuda, "Human-machine cooperative tele-manipulation with motion and force scaling using task-oriented virtual tool dynamics," *IEEE Trans. Robot. Autom.*, vol. 16, no. 5, pp. 505–516, Oct. 2000.
- [4] C. Monserrat, U. Meier, M. Alcañiz, F. Chinesta, and M. C. Juan, "A new approach for the real-time simulation of tissue deformations in surgery simulation," *Comput. Methods Programs Biomed.*, vol. 64, no. 2, pp. 77–85, Feb. 2001.
- [5] T. M. Martinetz, S. G. Berkovich, and K. J. Schulten, "Neural-gas network for vector quantization and its application to time-series prediction," *IEEE Trans. Neural Netw.*, vol. 4, no. 4, pp. 558–568, Jul. 1993.
- [6] N. Davey, R. G. Adams, and S. J. George, "The architecture and performance of a stochastic competitive evolutionary neural tree network," *Appl. Intell.*, vol. 12, no. 1/2, pp. 75–93, Jan. 2000.
- [7] B. Fritzke, "Unsupervised ontogenic networks," in *Handbook of Neural Computation*, E. Fiesler and R. Beale, Eds. London, U.K.: Oxford Univ. Press, 1997, ch. C2.4.
- [8] N. Kasabov, *Evolving Connectionist Systems: Methods and Applications in Bioinformatics, Brain Study and Intelligent Machines*. New York: Springer-Verlag, 2003.
- [9] —, *SOM Toolbox Online Documentation*, Laboratory of Computer and Information Science, Neural Network Research Centre, Helsinki University of Technology, Helsinki, Finland. [Online]. Available: <http://www.cis.hut.fi/project/somtoolbox/documentation/>
- [10] A.-M. Cretu, "Neural network modeling of 3D objects for virtualized reality applications," M.S. thesis, Dept. Elect. Comput. Eng., Univ. Ottawa, Ottawa, ON, Canada, 2003.
- [11] K. Keller and J. Ackerman, "Real-time structured light depth extraction," in *Proc. SPIE Photonics West—Three Dimensional Image Capture and Applications III*, San Jose, CA, Jan. 2000, pp. 11–18.
- [12] H. J. W. Spoelder, F. M. Vos, E. M. Petriu, and F. C. A. Groen, "Some aspects of pseudo random binary array based surface characterization," *IEEE Trans. Instrum. Meas.*, vol. 49, no. 6, pp. 1331–1336, Dec. 2000.
- [13] J. C. Carr, R. K. Beatson, J. B. Cherrie, T. J. Mitchell, W. R. Fright, B. C. McCallum, and T. R. Evans, "Reconstruction and representation of 3D objects with radial basis functions," in *Proc. Computer Graphics*, Los Angeles, CA, Aug. 2001, pp. 67–76.
- [14] D. L. James and D. K. Pai, "A unified treatment of elastostatic contact simulation for real time haptics," *Haptics-e—Electron. J. Haptics Res.*, vol. 2, no. 1, pp. 1–13, Sep. 2001.
- [15] G. Roth and M. D. Levine, "Minimal subset random sampling for pose determination and refinement," in *Advances in Machine Vision*, C. Archibald and E. Petriu, Eds. Singapore: World Scientific, 1992, pp. 1–21.



**Ana-Maria Cretu** (S'04) received the Master's degree from the School of Information Technology and Engineering, University of Ottawa, ON, Canada, in 2003, where she is currently pursuing the Ph.D. degree.

Her research interests include neural networks, tactile sensing, three-dimensional (3-D) object modeling, and multisensor data fusion.



**Emil M. Petriu** (M'86–SM'88–F'01) is a Professor and the University Research Chair in the School of Information Technology and Engineering, University of Ottawa, ON, Canada. His research interests include robot sensing and perception, intelligent sensors, interactive virtual environments, soft computing, and digital integrated circuit testing. He is the author or coauthor of more than 200 technical papers and two books, the Editor of another two books, and the holder of two patents.

Dr. Petriu is a Fellow of the Canadian Academy of Engineering and a Fellow of the Engineering Institute of Canada. He is a corecipient of IEEE's Donald G. Fink Prize Paper Award for 2003 and the recipient of the 2003 IEEE Instrumentation and Measurement Society Award. He is currently serving as Chair of the Technical Committee (TC)-15 Virtual Systems and the Cochair of TC-28 Instrumentation and Measurement for Robotics and Automation and TC-30 Security and Contraband Detection of the IEEE Instrumentation and Measurement Society. He is an Associate Editor of the IEEE TRANSACTIONS ON INSTRUMENTATION AND MEASUREMENT and a member of the Editorial Board of the *IEEE Instrumentation and Measurement (I&M) Magazine*.